

# First-Principles Study of Aziridinium Lead Iodide Perovskite for Photovoltaics

Qiang Teng,<sup>[a, b]</sup> Tingting Shi,<sup>[c]</sup> and Yu-Jun Zhao<sup>\*[a, b]</sup>

The long-term stability remains one of the main challenges for the commercialization of the rapidly developing hybrid organic-inorganic perovskite solar cells. Herein, we investigate the electronic and optical properties of the recently reported hybrid halide perovskite  $(\text{CH}_2)_2\text{NH}_2\text{PbI}_3$  (AZPbI<sub>3</sub>), which exhibits a much better stability than the popular halide perovskites  $\text{CH}_3\text{NH}_3\text{PbI}_3$  and  $\text{HC}(\text{NH}_2)_2\text{PbI}_3$ , by using density functional theory (DFT). We find that AZPbI<sub>3</sub> possesses a band gap of 1.31 eV, ideal for single-junction solar cells, and its optical absorption is compara-

ble with those of the popular  $\text{CH}_3\text{NH}_3\text{PbI}_3$  and  $\text{HC}(\text{NH}_2)_2\text{PbI}_3$  materials in the whole visible-light region. In addition, the conductivity of AZPbI<sub>3</sub> can be tuned from efficient *p*-type to *n*-type, depending on the growth conditions. Besides, the charge-carrier mobilities and lifetimes are unlikely hampered by deep transition energy levels, which have higher formation energies in AZPbI<sub>3</sub> according to our calculations. Overall, we suggest that the perovskite AZPbI<sub>3</sub> is an excellent candidate as a stable high-performance photovoltaic absorber material.

## 1. Introduction

In the past decade, organometallic lead halide perovskite has attracted significant attention as the absorbers in photovoltaics due to their outstanding properties, such as excellent carrier diffusion lengths, strong light absorption, high open-circuit voltages, low electron and hole effective masses, ambipolar charge transport, and solution processability.<sup>[1–7]</sup> Current lead perovskite solar cells can achieve high power conversion efficiencies (PCEs) up to NREL-certified 23.7%. The bulk of research has focused on methylammonium lead iodide  $\text{CH}_3\text{NH}_3\text{PbI}_3$  (MAPbI<sub>3</sub>), among the organometallic halide perovskites, owing to its unique photovoltaic properties and rapid improvements in PCEs in recent years. MAPbI<sub>3</sub> has a band gap of approximately 1.55 eV, which is slightly beyond the optimal value of ~1.3 eV for a single-junction solar cell.<sup>[1,8]</sup> The material, however, is sensitive to degradation under the moisture and high temperature conditions,<sup>[9–12]</sup> and thus limited in commercial application. Encapsulation of the MAPbI<sub>3</sub> solar cells hardly prevents their degradation either as the active layer of encapsulated hybrid organic perovskites often decomposes after a period of time that ranges from several days to a month.<sup>[13,14]</sup>

Alternatively, solar cells based on formamidinium lead triiodide  $\text{HC}(\text{NH}_2)_2\text{PbI}_3$  (FAPbI<sub>3</sub>) perovskites have been demon-

strated with a maximum power conversion efficiency of 20.1%.<sup>[15]</sup> Replacing cation MA with FA, a FAPbI<sub>3</sub> perovskite was found to possess a smaller band gap (1.48 eV), which allows better near-infrared absorption, and it has an elevated decomposition temperature and thus higher thermal stability.<sup>[16–19]</sup> Nevertheless, their stability cannot meet the requirement of commercialization either. In addition, deep levels often appear in FAPbI<sub>3</sub> due to intrinsic defects, which can act as non-radiative recombination centers and shorten the carrier lifetimes.<sup>[20]</sup> Thus, FAPbI<sub>3</sub>-based solar cells are hard to prevail their MAPbI<sub>3</sub> counterparts in PCEs.<sup>[17,21,22]</sup>


Recently, Zheng et al. reported that the ionization energy of the molecules on site A (in ABX<sub>3</sub> type perovskites) play a key role in stability, as the ionization energy has influence on the reaction enthalpy of halide perovskites.<sup>[23]</sup> Generally, low ionization energy of the molecules favors a stable perovskite structure. Subsequently, they theoretically proposed a three-membered cyclic organic cation-based hybrid halide perovskite AZPbI<sub>3</sub>, where the organic cation AZ demonstrates a low ionization that renders a good stability for AZPbI<sub>3</sub>.<sup>[24]</sup> Moreover, the size of AZ is slightly larger than MA and smaller FA, thus AZPbI<sub>3</sub> shows a smaller band gap which is more competent for the photovoltaic application. This implies that AZPbI<sub>3</sub> is a potential high efficiency absorber material for photovoltaics, and expect its electronic and optical properties, especially its defect physics behaving remarkable as the previous MA based perovskite systems.

Here, we systematically investigate the electronic and optical properties of AZPbI<sub>3</sub>, as well as its defect properties, based on first-principles calculations. It shows that the band gap of AZPbI<sub>3</sub> is optimal for PV applications (1.31 eV) and the optical absorption as well as carrier mobility is comparable with the popular MAPbI<sub>3</sub>. We suggest that AZPbI<sub>3</sub> can be a promising solar cell material, whose electrical properties can be tuned additionally from efficient *p*-type to *n*-type, depending on the growth condition.

[a] Dr. Q. Teng, Dr. Y.-J. Zhao  
Department of Physics, South China University of Technology, Guangzhou, Guangdong 510640, China  
E-mail: zhaoyj@scut.edu.cn

[b] Dr. Q. Teng, Dr. Y.-J. Zhao  
Key Laboratory of Advanced Energy Storage Materials of Guangdong Province, South China University of Technology, Guangzhou, Guangdong 510640, China

[c] Dr. T. Shi  
Siyuan Laboratory, Guangzhou Key Laboratory of Vacuum Coating Technologies and New Energy Materials, Department of Physics, Jinan University, Guangzhou, Guangdong 510632, China

 Supporting information for this article is available on the WWW under <https://doi.org/10.1002/cphc.201801033>

## 2. Computational Details

All calculations are performed using the Vienna *ab initio* simulation package (VASP)<sup>[25,26]</sup> based on the density functional theory with the projected augmented wave (PAW) method.<sup>[27,28]</sup> The valence electron configurations involved in the calculations are chosen as H (1  $s^1$ ), C (2  $s^2 2p^2$ ), N (2  $s^2 2p^3$ ), Pb (4d<sup>10</sup>5  $s^2 5p^2$ ), I (5  $s^2 5p^5$ ) and the exchange-correlation functional is described by the generalized gradient approximation (GGA) via the Perdew-Burke-Ernzerhof (PBE) functional.<sup>[29]</sup> GGA-PBE cannot describe the weak interaction between the organic and inorganic constituents in the hybrid perovskites well. This is ascribed to the fact that there is hydrogen bond formation between organic cations and inorganic matrix in hybrid organic-inorganic perovskites.<sup>[30]</sup> Meanwhile, the non-local van der Waals density functional (vdW-DF) has been demonstrated to describe hydrogen bonded systems reasonably.<sup>[31]</sup> Accordingly, the vdW-DF correction, as implemented in VASP by Klimes *et al.*<sup>[32,33]</sup> is adopted in our calculation. Previous study<sup>[24]</sup> indicated that due to the same Goldschmidt's tolerance factor 0.93, AZPbI<sub>3</sub> presumably have a similar atomic structure to the MAPbBr<sub>3</sub> case, which is a cubic structure at the room temperature.<sup>[34–36]</sup> Therefore, we adopt the cubic structure of AZPbI<sub>3</sub> with space group  $Pm\bar{3}m$  in our study. The initial structures of the cubic AZPbI<sub>3</sub> with the plan of three-membered cation oriented along (100) and (110) directions are constructed to start the structural optimization, and the lattice parameters as well as the atomic positions are fully relaxed until the Hellmann-Feynman force on each atom below 0.01 eV/Å. Monkhorst-Pack<sup>[37]</sup> scheme with  $6 \times 6 \times 6$  and  $8 \times 8 \times 8$   $\Gamma$ -centered for  $k$ -point sampling are chosen for the calculations of the structural optimization and electronic/properties, respectively. The wave function is expanded by plane-waves with energy cut-off at 520 eV. It is well known that PBE functional provides a reasonable band gap for MAPbI<sub>3</sub> due to the cancellation of errors from GGA and negligible of spin-orbital coupling (SOC) effect. Here, we have further applied the Heyd-Scuseria-Ernzerhof (HSE) hybrid functional<sup>[38]</sup> in combination with the SOC effect to study the electronic properties extensively. In our calculations, the mixing rate ( $\mu$ ) of the Hartree-Fock exchange potential is set to 0.43, yielding an excellent agreement on the band gap between the calculation and experiment for the MAPbI<sub>3</sub> phase with tetragonal crystal symmetry ( $I4cm$ ). In analogy, the HSE ( $\mu = 0.43$ ) including SOC is adopted for the cubic AZPbI<sub>3</sub>, giving the calculated band gaps of 1.31 and 1.59 eV for the cubic AZPbI<sub>3</sub> and the tetragonal MAPbI<sub>3</sub>, respectively. The former is consistent with available theoretical result of 1.35–1.49 eV<sup>[24]</sup> and the latter is in agreement with the experimental one, 1.55 eV.<sup>[1]</sup>

Based on the accurate electronic structure, the imaginary part  $\varepsilon_2(\omega)$  of the dielectric function dependence on the incidence optical frequency can be acquired, and the real part  $\varepsilon_1(\omega)$  can be estimated through the Kramers-Kronig transformation. The optical absorption coefficient  $I(\omega)$  can be obtained according to the following equation:<sup>[39]</sup>

$$I(\omega) = \sqrt{2}\omega[\sqrt{\varepsilon_1^2(\omega) + \varepsilon_2^2(\omega)} - \varepsilon_1(\omega)]^{1/2} \quad (1)$$

For the defect calculations, a  $3 \times 3 \times 3$  supercell containing 351 atoms is employed, with the corresponding Brillouin zone sampled by the  $\Gamma$  point. The atomic coordinates are relaxed until the force on each atom is below 0.05 eV/Å. The defect formation energy  $\Delta H(\alpha, q)$  has been calculated using the following equation<sup>[40]</sup>

$$\Delta H(\alpha, q) = E(\alpha, q) - E_h + \sum_i n_i(E_i + \Delta\mu_i) + q[E_v + E_f + \Delta V] \quad (2)$$

Here  $E(\alpha, q)$  is the total energy of the supercell containing the defect  $\alpha$  in charge state  $q$  and  $E_h$  is the perfect supercell one.  $n_i$  represents the number of  $i$  atom, which is positive when the atom removed from supercell and negative when added to the supercell in forming the defect.  $\Delta\mu_i$  is the relative chemical potential of  $i$  depending on the experimental conditions and  $E_i$  is the total energy of  $i$  as pure elemental solid or molecule.  $E_v$  is the valance band maximum (VBM) energy of the host material and  $E_f$  is the Fermi energy referred to the VBM. In contrast to charge-neutral systems, the total energy in charged systems can not be well defined. Thus, the potential alignment correction is considered to correct the systems with different charged states.<sup>[40]</sup> The average electrostatic potential at the atomic sites far from the defect is aligned with that in the ideal crystal, and the resulting difference  $\Delta V$  is added in the Eq. (2). The transition level of the defect  $\varepsilon(q/q')$  is defined as the Fermi level at which the formation energies of defect  $\alpha$  with charge states  $q$  and  $q'$  are equal<sup>[40]</sup>

$$\varepsilon_q^q = [\Delta H(\alpha, q) - \Delta H(\alpha, q')]/(q' - q) \quad (3)$$

where  $\Delta H(\alpha, q)$  and  $\Delta H(\alpha, q')$  are the formation energies of defect  $\alpha$  with charge states  $q$  and  $q'$ , respectively.

## 3. Results and Discussion

### 3.1. Structural Properties

The cubic structure with space group  $Pm\bar{3}m$  is adopted for AZPbI<sub>3</sub> and the optimized atomic structure, which is consistent with the previous study,<sup>[24]</sup> is illustrated in Figure 1(a). The aziridinium (AZ) radical is a three-membered ring organic cation, which is a promising candidate to be used as the organic cation at site A of hybrid halide perovskites. The three-membered ring of the AZ cation consists of a C–C bond and two C–N bonds, where both of the C atoms have two chemical bond formations C–C and C–N bonds, and the N atom has double C–N bonds. These chemical bond formations strengthen the interaction between the two C atoms and N atom. This suggests that the three-membered ring is energetically unfavorable to break. Besides, the decomposition enthalpy of AZ was calculated by zheng *et al.*, which indicates that the AZ cation

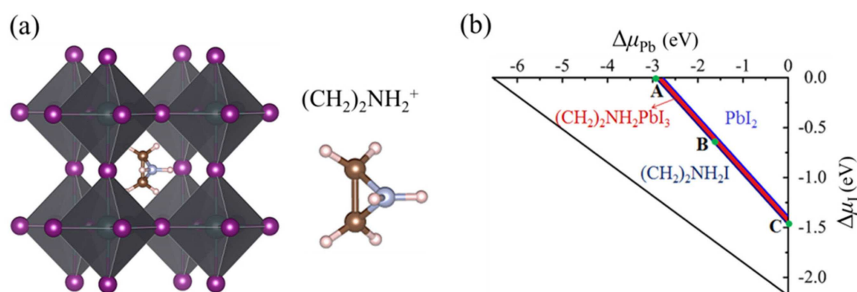


**Figure 1.** a) Schematic perovskite structure of AZPbI<sub>3</sub>. b) The thermodynamic stability range of equilibrium for AZPbI<sub>3</sub> is represented by the red-color region. Outside this region, the compound will decompose into PbI<sub>2</sub> or AZI. The representative points A ( $\mu_{\text{AZ}} = -3.61$  eV,  $\mu_{\text{Pb}} = -2.94$  eV,  $\mu_{\text{I}} = 0$  eV), B ( $\mu_{\text{AZ}} = -2.95$  eV,  $\mu_{\text{Pb}} = -1.50$  eV,  $\mu_{\text{I}} = 0.70$  eV), C ( $\mu_{\text{AZ}} = -2.05$  eV,  $\mu_{\text{Pb}} = 0$  eV,  $\mu_{\text{I}} = -1.47$  eV) are chosen for further investigation of defect properties (c.f. Figure 3).

can be stable in an aqueous solution.<sup>[24]</sup> The three-membered ring cation is slightly larger than MA, while smaller than FA. The calculated lattice constant  $a$  is 6.42 Å, slightly larger than cubic MAPbI<sub>3</sub>.

As well known, formability of inorganic perovskite structures can be rationalized via geometrical factors, such as the Goldschmidt's tolerance factor and Paulings's octahedral factor. To calculate the geometrical factors of hybrid halide perovskites, the effective organic cation radii are estimated as proposed by Kieslich et al.<sup>[41]</sup> The size of cyclic cations is between that of MA and FA. The tolerance of factor for AZPbI<sub>3</sub> is 0.93, which is within the perovskite formability limits.<sup>[42]</sup> Nevertheless, the tolerance factor and octahedral factor are insufficient to predict the formability and stability of organic-inorganic hybrid perovskites.<sup>[43]</sup> Zheng et al. pointed out that the ionization energy of organic cation in organic-inorganic hybrid perovskites has effect on the stability of the perovskites.<sup>[23,24]</sup> Lower ionization energies of the cations render more stable structure. This can be explained that the ionization energy of organic cation in hybrid perovskites has a contribution to the decomposition energy of the perovskites, where low ionization energy leads to an remarkably unfavorable decomposition energy. These reports indicated that AZPbI<sub>3</sub> has lower decomposition energy than both mainstream perovskites MAPbI<sub>3</sub> and FAPbI<sub>3</sub> due to the lower ionization in organic cation.

Here, the decomposition energy  $\Delta H_r$  of AZPbI<sub>3</sub> is calculated by following decomposition reaction equation



and the corresponding enthalpy

$$\Delta H_r = E_{\text{tot}}[\text{AZPbI}_3] - E_{\text{tot}}[\text{AZI}] - E_{\text{tot}}[\text{PbI}_2] \quad (5)$$

Our calculated  $\Delta H_r$  is −31 meV/unit-cell, which is agreement with previous report.<sup>[24]</sup>

In thermodynamic equilibrium growth condition, the existence of AZPbI<sub>3</sub> should satisfy

$$\mu_{\text{AZ}} + \mu_{\text{Pb}} + 3\mu_{\text{I}} = \Delta H(\text{AZPbI}_3) = -6.55 \text{ eV} \quad (6)$$

where  $\mu_i$  is the chemical potential of constitute element referred

to its most stable phase and  $\Delta H$  AZPbI<sub>3</sub> is the formation enthalpy of AZPbI<sub>3</sub>. For  $\mu_{\text{AZ}}$ , we choose face-centered-cubic phase of AZ following bulk Cs. To exclude the possible secondary phase PbI<sub>2</sub> and AZI (rock-salt phase), the following constraints must also be satisfied:

$$\mu_{\text{AZ}} + \mu_{\text{I}} < \Delta H(\text{AZI})(-3.61 \text{ eV}) \quad (7)$$

$$\mu_{\text{Pb}} + 2\mu_{\text{I}} < \Delta H(\text{PbI}_2)(-2.77 \text{ eV}) \quad (8)$$

The chemical potentials of Pb and I satisfying Eqs. (6)–(8) are shown in the red region of Figure 1(b), in which AZPbI<sub>3</sub> is stable against possible competing phases including Pb, I<sub>2</sub>, AZI and PbI<sub>2</sub>. The stable chemical potential window for AZPbI<sub>3</sub> has a long but narrow shape, typical for halide perovskites, indicating that the chemical growth condition should be carefully controlled to form pure AZPbI<sub>3</sub>.

Recently, Zhang et al.<sup>[44]</sup> calculated the MAPbI<sub>3</sub> phase-separation energy using first-principles calculations, and found it was negative, in line with the experiment results.<sup>[45]</sup> Yin et al.,<sup>[46]</sup> however, reported that the MAPbI<sub>3</sub> was available in a narrow thermodynamic stable range, in contrary to the above recent studies.<sup>[46]</sup> This is attributed to the fact that the hypothetical NaCl phase was adopted for MAI by Yin et al, and the decomposition enthalpy was overestimated. Accordingly, AZPbI<sub>3</sub> perovskite is expected to be more stable than MAPbI<sub>3</sub>, although the stable range for AZPbI<sub>3</sub> is rather narrow (c.f. Figure 1 (b)).

### 3.2. Electronic Properties

To study the light harvesting effect of AZPbI<sub>3</sub>, its electronic structure is also investigated. The calculated band structure of the AZPbI<sub>3</sub> using HSE06 functional with considering of SOC is shown in left panel of Figure 2a. The calculated band gap is 1.31 eV, which is in agreement with previous theoretical results of 1.35–1.53 eV.<sup>[24]</sup> Furthermore, the band gap of AZPbI<sub>3</sub> is optimal for realizing high PV performance solar cell, as the Shockley-Queisser limit suggests a band gap of ~1.3 eV for achieving maximum PCE in a single  $p$ - $n$  junction solar cell.<sup>[8]</sup> Compared with the popular MAPbI<sub>3</sub> (with band gap of

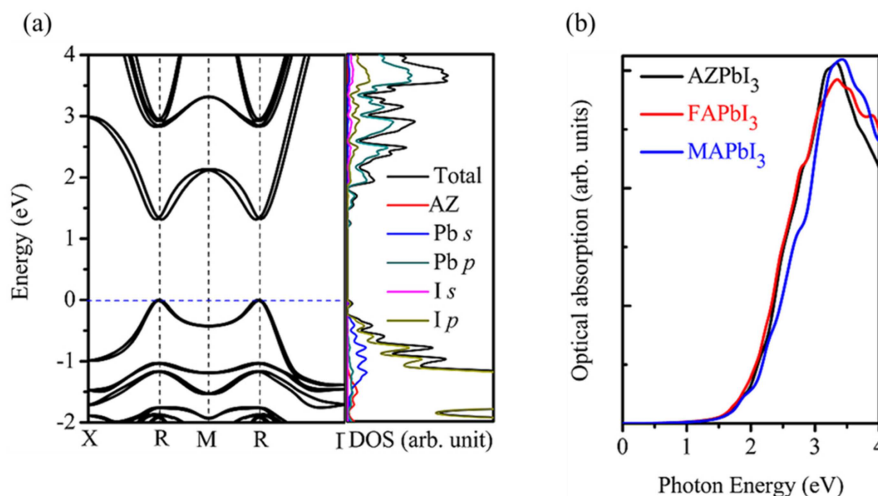


**Figure 2.** a) Calculated band structure of AZPbI<sub>3</sub> based on the cubic phase using the HSE06 functional with SOC. Here, the VBM is set to zero. b) Calculated optical absorption spectra of MAPbI<sub>3</sub>, FAPbI<sub>3</sub>, and AZPbI<sub>3</sub> using the HSE06 functional with SOC.

~1.50 eV), AZPbI<sub>3</sub> has a potential for achieving superior PV performance. It should be noted that there is an unobvious split in the conduction band minimum (CBM) of AZPbI<sub>3</sub> (c.f. Figure 2a). This could be due to the strong spin-orbit interaction and distortions in the Pb-centered octahedron, a Rashba splitting at the vicinity of the band extreme as reported in MAPbI<sub>3</sub>.<sup>[47–49]</sup> The Rashba splitting leads to an effectively indirect band gap. The projected density of states (PDOS) is also shown in the right panel in Figure 2a. It is obvious that the organic cation AZ has little contribution to the energy bands around VBM and CBM. The VBM of AZPbI<sub>3</sub> is mainly contributed by the *p* orbital of the I atoms and partly contributed by the *s* orbital of the Pb atoms, involving strong anti-bonding coupling, while the CBM is dominated by *p* orbitals of the Pb atoms, in analogy to FAPbI<sub>3</sub> and MAPbI<sub>3</sub>. This implies that AZPbI<sub>3</sub> could inherit the excellent PCE performance from MAPbI<sub>3</sub> and FAPbI<sub>3</sub>, with the widely dispersed *s*, *p* levels dominating VBM and CBM.

Moreover, the absorption spectrum of the AZPbI<sub>3</sub> is also calculated, and it is compared with the absorption spectra of two popular perovskite solar cell materials MAPbI<sub>3</sub> and FAPbI<sub>3</sub> shown in Figure 2b. Our calculations show that the shapes of the three considered structures curves are quite close to each other, implying that AZPbI<sub>3</sub> has comparable absorption ability with MAPbI<sub>3</sub> and FAPbI<sub>3</sub> in the whole visible region. Besides, the corresponding spectrum of the MAPbI<sub>3</sub> is slightly blue shifted with respect to that of AZPbI<sub>3</sub> and FAPbI<sub>3</sub>. This agrees with the trend of the band gaps of above three compounds.

Meanwhile, light effective masses are also expected to facilitate the transportation of the photo-generated electrons and holes, which will be thermally relaxed to the CBM and VBM, respectively. The corresponding calculated effective masses are listed in Table 1, showing that (i) the electron and hole effective masses are balanced, thus AZPbI<sub>3</sub> has a good bipolar conductivity; (ii) both the electron and hole effective masses of AZPbI<sub>3</sub> are rather light, comparable to that of MAPbI<sub>3</sub>. These

features indicate that AZPbI<sub>3</sub> has high carrier mobility as MAPbI<sub>3</sub>.

### 3.3. Intrinsic Defect Properties

The photovoltaic properties of an absorber can be largely affected by the intrinsic defects. Here we have considered 12 possible intrinsic point defects in AZPbI<sub>3</sub>, including three types of vacancies (*V<sub>I</sub>*, *V<sub>Pb</sub>*, and *V<sub>AZ</sub>*), three types of interstitials (*I<sub>I</sub>*, *I<sub>Pb</sub>*, and *I<sub>AZ</sub>*), two cation substitutions (*Pb<sub>AZ</sub>* and *AZ<sub>Pb</sub>*), and four antisite substitutions (*I<sub>Pb</sub>*, *I<sub>AZ</sub>*, *Pb<sub>I</sub>*, and *AZ<sub>I</sub>*). Considering the thermodynamic equilibrium growth conditions, the formation energies of point defects are mostly dependent on the chemical potentials of the host elements,  $\mu_I$ ,  $\mu_{Pb}$  and  $\mu_{AZ}$ . A moderate chemical potential region is identified for achieving thermodynamically stable AZPbI<sub>3</sub>. The identified chemical potential region for AZPbI<sub>3</sub> is highlighted in red in Figure 1b. Here we calculated the formation energies as a function of the Fermi level under three extreme cases (c.f. Figure 1b): (A) I-rich/Pb-poor, (B) moderate and (C) I-poor/Pb-rich conditions, as plotted in Figure 3.

The calculated results show that the conductivity of AZPbI<sub>3</sub> can be tuned from intrinsic good *p*-type, moderate, to good *n*-type when the sample preparation condition shifts from A (I-rich/Pb-poor), B (moderate), to C (I-poor/Pb-rich). Such flexible defect properties are similar to that in MAPbI<sub>3</sub>.<sup>[46]</sup>

Under the I-rich and Pb-poor conditions, the acceptor defects *V<sub>Pb</sub>*, *I<sub>Pb</sub>*, *I<sub>I</sub>* and *I<sub>AZ</sub>*, and donor defect *V<sub>I</sub>* have relatively low formation energies, with the Fermi level pinned at 0.03 eV above the VBM by *V<sub>Pb</sub>* and *V<sub>I</sub>*. In this case, the AZPbI<sub>3</sub> exhibits excellent *p*-type conductivity. The conductivity is expected to be much better than the intrinsic *p*-type conductivity of MAPbI<sub>3</sub>,<sup>[46]</sup> in consideration of shallow Fermi level. The formation energies of the *V<sub>Pb</sub>* in AZPbI<sub>3</sub> are relative higher than that in MAPbI<sub>3</sub>, largely due to the weaker antibonding state at VBM of

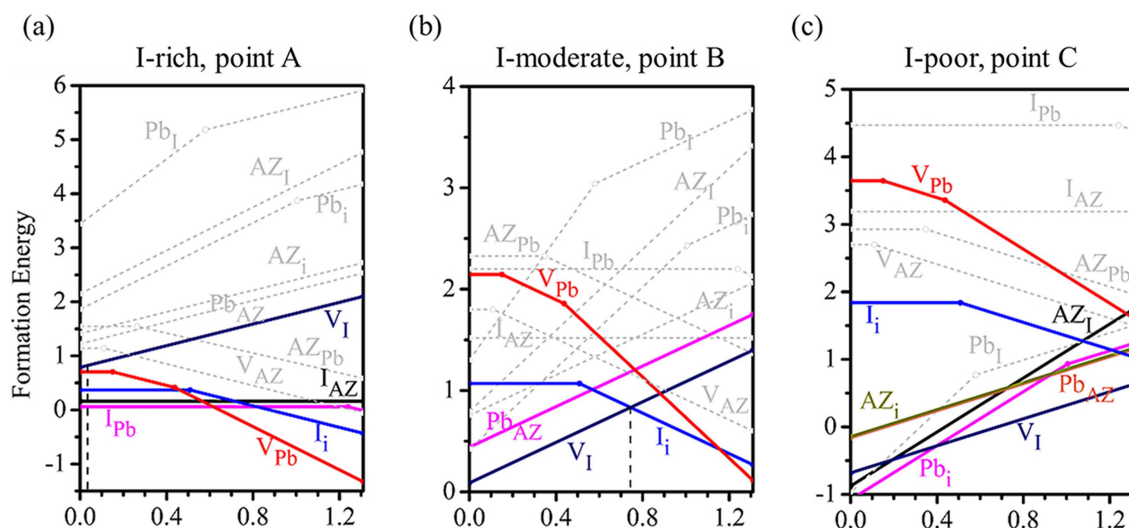


**Figure 3.** The formation energies of intrinsic point defects under: a) I-rich b) moderate, and c) Pb-rich conditions. Defects with high formation energies are displayed as dashed lines.

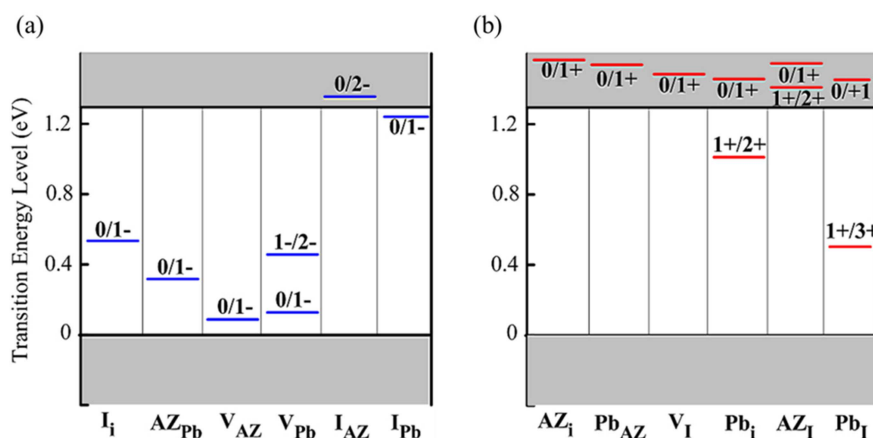


**Figure 4.** Calculated transition energy levels for: a) intrinsic acceptors and b) intrinsic donors in AZPbI<sub>3</sub>.

AZPbI<sub>3</sub> than that in MAPbI<sub>3</sub>. Due to the formation of covalent I dimers the interstitial defect I<sub>i</sub> also has low formation energies.

As the growth condition shifts from I-rich/Pb-poor (point A) to I/Pb moderate (point B), the formation energies of acceptor defects increase, while the donor defects are easier to form, as V<sub>I</sub> and I<sub>i</sub> are the dominant donor and acceptor, respectively. Subsequently, Fermi level is pinned at 0.75 eV above the VBM by V<sub>I</sub> and I<sub>i</sub>, and thus AZPbI<sub>3</sub> becomes either intrinsic or slightly *n*-type conductivity. At the growth condition of point C, I-poor/Pb-rich, the formation energies of acceptor defects continue to increase, and the donor defects become dominant. Under this growth condition, the Fermi level is inside the CBM, dominated by V<sub>I</sub>, indicating a degenerately doping with excellent *n*-type conductivity. It can be seen that the *n*-type conductivity of AZPbI<sub>3</sub> is due to the low formation energy of V<sub>I</sub>, while those of MAPbI<sub>3</sub> and FAPbI<sub>3</sub> are attributed to dominant donor defect MA<sub>i</sub> and FA<sub>i</sub>, respectively.<sup>[20,46]</sup> Overall, we conclude that the

organic cations have remarkable effect on the defect properties of halide perovskites.

Defects with deep transition levels in the band gap can act as Shockley-Read-Hall recombination centers. In addition, the scattering effect of charged defects will affect carrier migration and reduce the conductivity. Both the effects have a major impact on the device performance. The HSE-SOC calculated transition energy levels of all possible intrinsic defects are plotted relative to the VBM and CBM, as shown in Figure 4. It can be seen that all the acceptor defects, donor defects Pb<sub>i</sub> and Pb<sub>i</sub> would introduce deep transition levels. All other defects have shallow transition levels. Though all acceptor defects can create deep transition levels, most of them have relatively high formation energies, preventing them from being an effective recombination center. In addition, defect I<sub>i</sub> is of low formation energy but stabilized in neutral charge state under the I-rich/Pb-poor condition. In contrast, defect I<sub>i</sub> has relatively low formation energy and induces deep transition levels under

mediate and I-poor/Pb-rich conditions. Consequently, we suggest that the AZPbI<sub>3</sub> films should be synthesized under the I-rich/Pb-poor conditions in order to suppress the formation deep defects and optimize the photovoltaic performance.

## 4. Conclusions

To summarize, we have systematically studied the electronic and all possible intrinsic point defect of AZPbI<sub>3</sub> perovskite by DFT calculations. We find that the good stability hybrid halide perovskite AZPbI<sub>3</sub> possess excellent electronic and optical properties as visible-light absorber materials for PV applications, comparable with the popular MAPbI<sub>3</sub> material. Moreover, like MAPbI<sub>3</sub> perovskite, the electrical conductivity can be tuned from p-type to n-type efficiently, by changing the synthesis conditions. Deep transition levels from intrinsic defects are hardly expected to appear in AZPbI<sub>3</sub>, favoring its high PCE. Overall, the perovskite AZPbI<sub>3</sub> is suggested to be an excellent candidate for solar cells with both high stability and performance.

## Acknowledgments

This work is financially supported by NSFC (Grant Nos. 11574088 and 51431001), the Foundation for Innovative Research Groups of the National Natural Science Foundation of China (Grant No. 51621001), and Natural Science Foundation of Guangdong Province of China (Grant No. 2016A030312011).

## Conflict of Interest

The authors declare no conflict of interest.

**Keywords:** density functional calculation · electronic property · lead halide perovskite · photovoltaic · solar cell

- [1] A. Kojima, K. Teshima, Y. Shirai, T. Miyasaka, *J. Am. Chem. Soc.* **2009**, *131*, 6050.
- [2] H.-S. Kim, C.-R. Lee, J.-H. Im, K.-B. Lee, T. Moehl, A. Marchioro, S.-J. Moon, R. Humphry-Baker, J.-H. Yum, J. E. Moser, M. Grätzel, N.-G. Park, *Sci. Rep.* **2012**, *2*, 591.
- [3] S. D. Stranks, G. E. Eperon, G. Grancini, C. Menelaou, M. J. P. Alcocer, T. Leijtens, L. M. Herz, A. Petrozza, H. J. Snaith, *Science* **2013**, *342*, 341.
- [4] S. De Wolf, J. Holovsky, S.-J. Moon, P. Löper, B. Niesen, M. Ledinsky, F.-J. Haug, J.-H. Yum, C. Ballif, *J. Phys. Chem. Lett.* **2014**, *5*, 1035–1039.
- [5] C. Wehrenfennig, G. E. Eperon, M. B. Johnston, H. J. Snaith, L. M. Herz, *Adv. Mater.* **2014**, *26*, 1584–1589.
- [6] G. Xing, N. Mathews, S. Sun, S. S. Lim, Y. M. Lam, M. Grätzel, S. Mhaisalkar, T. C. Sum, *Science* **2013**, *342*, 344.
- [7] W. Wang, M. O. Tadé, Z. Shao, *Chem. Soc. Rev.* **2015**, *44*, 5371–5408.
- [8] W. Shockley, *Czech. J. Phys.* **1961**, *11*, 81–121.
- [9] Z. Song, A. Abate, S. C. Watthage, G. K. Liyanage, A. B. Phillips, U. Steiner, M. Graetzel, M. J. Heben, *Adv. Energy Mater.* **2016**, *6*, 1600846.
- [10] S. Wozny, M. Yang, A. M. Nardes, C. C. Mercado, S. Ferrere, M. O. Reese, W. Zhou, K. Zhu, *Chem. Mater.* **2015**, *27*, 4814–4820.
- [11] A. Buin, R. Comin, J. Xu, A. H. Ip, E. H. Sargent, *Chem. Mater.* **2015**, *27*, 4405–4412.
- [12] T. Xu, L. Chen, Z. Guo, T. Ma, *Phys. Chem. Chem. Phys.* **2016**, *18*, 27026–27050.
- [13] J. Burschka, N. Pellet, S. J. Moon, R. Humphry-Baker, P. Gao, M. K. Nazeeruddin, M. Grätzel, *Nature* **2013**, *499*, 316.
- [14] Y. Han, S. Meyer, Y. Dkhissi, K. Weber, J. M. Pringle, U. Bach, L. Spiccia, Y.-B. Cheng, *J. Mater. Chem. A* **2015**, *3*, 8139–8147.
- [15] W. S. Yang, J. H. Noh, N. J. Jeon, Y. C. Kim, S. Ryu, J. Seo, S. I. Seok, *Science* **2015**, *348*, 1234.
- [16] S. Pang, H. Hu, J. Zhang, S. Lv, Y. Yu, F. Wei, T. Qin, H. Xu, Z. Liu, G. Cui, *Chem. Mater.* **2014**, *26*, 1485–1491.
- [17] G. E. Eperon, S. D. Stranks, C. Menelaou, M. B. Johnston, L. M. Herz, H. J. Snaith, *Energy Environ. Sci.* **2014**, *7*, 982–988.
- [18] T. M. Koh, K. Fu, Y. Fang, S. Chen, T. C. Sum, N. Mathews, S. G. Mhaisalkar, P. P. Boix, T. Baikie, *J. Phys. Chem. C* **2014**, *118*, 16458–16462.
- [19] N. Pellet, P. Gao, G. Gregori, T.-Y. Yang, M. K. Nazeeruddin, J. Maier, M. Grätzel, *Angew. Chem.* **2014**, *126*, 3215–3221; *Angew. Chem. Int. Ed.* **2014**, *53*, 3151–3157.
- [20] N. Liu, C. Yam, *Phys. Chem. Chem. Phys.* **2018**, *20*, 6800–6804.
- [21] D.-J. Seol, J.-W. Lee, N.-G. Park, *ChemSusChem* **2015**, *8*, 2414–2419.
- [22] J.-W. Lee, D.-J. Seol, A.-N. Cho, N.-G. Park, *Adv. Mater.* **2014**, *26*, 4991–4998.
- [23] C. Zheng, O. Rubel, *J. Phys. Chem. C* **2017**, *121*, 11977–11984.
- [24] C. Zheng, O. Rubel, *J. Phys. Chem. Lett.* **2018**, *9*, 874–880.
- [25] G. Kresse, J. Furthmüller, *Comp. Mater. Sci.* **1996**, *6*, 15–50.
- [26] G. Kresse, J. Furthmüller, *Phys. Rev. B* **1996**, *54*, 11169–11186.
- [27] G. Kresse, D. Joubert, *Phys. Rev. B* **1999**, *59*, 1758–1775.
- [28] P. E. Blöchl, *Phys. Rev. B* **1994**, *50*, 17953–17979.
- [29] J. P. Perdew, K. Burke, M. Ernzerhof, *Phys. Rev. Lett.* **1996**, *77*, 3865.
- [30] W. Geng, L. Zhang, Y.-N. Zhang, W.-M. Lau, L.-M. Liu, *J. Phys. Chem. C* **2014**, *118*, 19565–19571.
- [31] M. Dion, H. Rydberg, E. Schröder, D. C. Langreth, B. I. Lundqvist, *Phys. Rev. Lett.* **2004**, *92*, 246401.
- [32] K. Lee, E. D. Murray, L. Kong, B. I. Lundqvist, D. C. Langreth, *Phys. Rev. B* **2010**, *82*, 081101.
- [33] K. Jiří, R. B. David, M. Angelos, *J. Phys. Condens. Matter* **2010**, *22*, 022201.
- [34] G. P. Nagabhushana, R. Shivaramaiah, A. Navrotsky, *Proc. Mont. Acad. Sci. USA* **2016**, *113*, 7717–7721.
- [35] A. Poglitsch, D. Weber, *J. Chem. Phys.* **1987**, *87*, 6373–6378.
- [36] N. Onoda-Yamamuro, T. Matsuo, H. Suga, *J. Phys. Chem. Solids* **1990**, *51*, 1383–1395.
- [37] H. J. Monkhorst, J. D. Pack, *Phys. Rev. B* **1976**, *13*, 5188–5192.
- [38] J. Paier, M. Marsman, K. Hummer, G. Kresse, I. C. Gerber, J. G. Ángyán, *J. Chem. Phys.* **2006**, *124*, 154709.
- [39] S. Saha, T. P. Sinha, A. Mookerjee, *Phys. Rev. B* **2000**, *62*, 8828–8834.
- [40] S. Lany, A. Zunger, *Phys. Rev. B* **2008**, *78*, 235104.
- [41] G. Kieslich, S. Sun, A. K. Cheetham, *Chem. Sci.* **2014**, *5*, 4712–4715.
- [42] L. M. Feng, L. Q. Jiang, M. Zhu, H. B. Liu, X. Zhou, C. H. Li, *J. Phys. Chem. Solids* **2008**, *69*, 967–974.
- [43] C. Li, K. C. K. Soh, P. Wu, *J. Alloys Compd.* **2004**, *372*, 40–48.
- [44] Z. Yue-Yu, C. Shiyu, X. Peng, X. Hongjun, G. Xin-Gao, W. Aron, W. Su-Huai, *Chinese Phys. Lett.* **2018**, *35*, 036104.
- [45] B. Conings, J. Drijkoningen, N. Gauquelin, A. Babayigit, J. D'Haen, L. D'Olieslaeger, A. Ethirajan, J. Verbeeck, J. Manca, E. Mosconi, F. D. Angelis, H.-G. Boyen, *Adv. Energy Mater.* **2015**, *5*, 1500477.
- [46] W.-J. Yin, T. Shi, Y. Yan, K. A., T. K., S. Y., M. T., *Appl. Phys. Lett.* **2014**, *104*, 063903.
- [47] J. Even, L. Pedesseau, J.-M. Jancu, C. Katan, *J. Phys. Chem. Lett.* **2013**, *4*, 2999–3005.
- [48] F. Brivio, K. T. Butler, A. Walsh, M. van Schilfgaarde, *Phys. Rev. B* **2014**, *89*, 155204.
- [49] F. Zheng, L. Z. Tan, S. Liu, A. M. Rappe, *Nano Lett.* **2015**, *15*, 7794–7800.
- [50] Y. Yin, Y. Huang, Y. Wu, G. Chen, W.-J. Yin, S.-H. Wei, X. Gong, *Chem. Mater.* **2017**, *29*, 9429–9435.

Manuscript received: November 7, 2018

Revised manuscript received: December 13, 2018

Accepted manuscript online: December 15, 2018

Version of record online: December 15, 2018